ESTIMATING TIME-DEPENDENT RESERVOIR PROPERTIES BY ANALYZING LONG-TERM PRESSURE DATA

A REPORT SUBMITTED TO THE DEPARTMENT OF PETROLEUM ENGINEERING

OF STANFORD UNIVERSITY

IN PARTIAL FULFILLMENT OF THE REQUIREMENTS FOR THE DEGREE OF MASTER OF SCIENCE

By
Jang Hyun Lee
June 2003

I certify that I have read this report and that in my opinion it is fully adequate, in scope and in quality, as partial fulfillment of the degree of Master of Science in Petroleum Engineering.

_____

Prof. Roland Horne
(Principal Advisor)

Abstract

Traditionally, well testing has been carried out over a specified time period. The resulting data have been the basis of the analysis of the reservoir. However, more recently, many completed wells have a permanent downhole gauge, from which continuous long-term data are recorded. From this long-term data, we can find that some of reservoir parameters, which were regarded as constants in traditional well testing, might change. In this research, changing permeability and skin factor were considered. With permeability and skin factor changing over time, a new analytical solution was developed. The new analytical solution was verified with numerical simulation results. This solution was applied to real reservoir data recorded from a permanent downhole gauge using an inverse simulation. The results showed that this solution is consistent with real reservoir data.

Acknowledgments

I would like to express my gratitude toward Professor Roland N. Horne for his continuous guidance, advice, encouragement and tremendous patience throughout the course of the study.

I would like to thank my colleagues in the SUPRI-D research group for their suggestions and comments in this project.

I am really grateful to my parents, my sister and brother-in-law, grandmother, and my fiancée, Ji Eun and her parents for their continuous support and encouragement during my studies. Also, I thank all of my friends.

I would also like to thank member companies of the SUPRI-D Research Consortium for Innovation in Well Test Analysis for providing financial support for this work.

Thank you, God.

Contents

List of Tables

List of Figures

Chapter 1

1. Introduction

We use mathematical reservoir models to describe reservoirs. The reservoir models require several parameters: permeability, skin factor, and so on. These models are calibrated using well test data consisting mainly of production and pressure data over time. These data are measured through well testing.

Using production and pressure data, engineers determine parameters by fitting the data to the model equations. Traditionally, well testing has been carried over a short time period. In well testing, reservoir parameters have been regarded as constant in time, for example permeability and skin factor. However, in reality, these parameters may not be constant, since reservoir conditions may change in time. It is reasonable that analysis of short-term data recorded from well testing can consider that such parameters are constant, since these parameters may change only very slowly in time. Now, however, long-term data can be recorded from a permanent downhole gauge. Long-term data can show the change of reservoir parameter values. This means that the analysis tools with constant parameters are inappropriate to apply to long-term data, and new modeling tools are required.

1.1. Problem Statement

There have been several studies to develop methods for analyzing long-term pressure data. Athichanagorn (1999) and Khong (2001) showed that the estimated permeability and skin factor changed over time in the long-term data recorded from a permanent downhole gauge in a North Sea oil field. Figure 1.1, which is from the study of Khong (2001), shows this changing permeability. However, the solutions made use of constant property assumptions, which is not mathematically correct, and the permeability estimates change abruptly, which is unrealistic. Unfortunately, there is no analytical reservoir pressure solution yet for changing permeability. Therefore, a new set of analytical solutions is needed to process this long-term data.

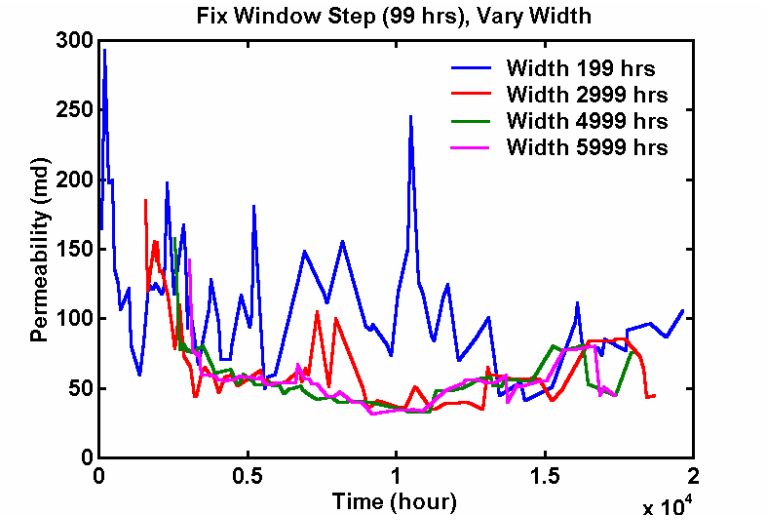

Figure 1.1: Changing permeability estimates (Khong, 2001).

1.2. Outline of Research

To overcome this problem, we derived a mathematical solution including time-dependent permeability and skin factor. To check the reliability of this solution, we carried out comparisons between the pressure values from the new analytical solution and numerical simulation results using a commercial numerical simulator. Subsequently, we analyzed real reservoir data using the new analytical solution.

Chapter 2

2. New Mathematical Solution

As noted in the previous chapter, Athichanagorn (1999) and Khong (2001) used long-term data from permanent downhole gauges to show that permeability might change in time. They used moving window approach, but this resulted in unrealistically abrupt changes of permeability estimates. The use of superposition of constant-property solutions in this case was not very clear from the point of view of mathematical correctness. Therefore, a new analytical solution accounting explicitly for time-dependent properties was needed.

2.1. Assumptions

There are two assumptions:

- Permeability changes with time.
- The rate of change of permeability is very slow.

2.2. Governing Equation and Boundary Conditions

Variable p is the difference between initial pressure and well bottom hole flowing pressure:

$$p = p_i - p_{wf} \tag{2.1}$$

$$\frac{1}{r}\frac{\partial}{\partial r}(k(t)r\frac{\partial p}{\partial r}) = \frac{\phi\mu c_t}{\alpha_2}\frac{\partial p}{\partial t} \tag{2.2}$$

There is an initial condition:

$$p(r, t=0) = 0 \tag{2.3}$$

There are two boundary conditions, one of which is for the well, the other of which is for the reservoir boundary.

$$-q = \lim_{r\to 0}\frac{2\pi k(t)h}{\alpha_1 B\mu}r\frac{\partial p}{\partial r} \tag{2.4}$$

$$p(r=\infty, t) = 0 \tag{2.5}$$

2.3. Solving the Partial Differential Equation

Permeability is a function of time $k(t)$. Because the function of permeability $k(t)$ is independent of r, it can be put on the right hand side of Equation (2.2).

$$\frac{1}{r}\frac{\partial}{\partial r}\left(r\frac{\partial p}{\partial r}\right)=\frac{\phi\mu c_t}{k(t)\alpha_2}\frac{\partial p}{\partial t} \tag{2.6}$$

To apply the well boundary condition, p^* is defined as:

$$p^*=\frac{k(t)}{k_0}p \tag{2.7}$$

Therefore, the original equation is changed as follows, with p^* substituted for p:

$$\frac{1}{r}\frac{\partial}{\partial r}\left(r\frac{\partial p^*}{\partial r}\right)=\frac{\phi\mu c_t}{\alpha_2 k(t)}\frac{\partial p^*}{\partial t}-\frac{\phi\mu c_t}{\alpha_2}p^*\frac{1}{(k(t))^2}\frac{\partial k(t)}{\partial t} \tag{2.8}$$

From the assumption that $k(t)$ is changing only very slowly in time, $\frac{\partial k(t)}{\partial t}$ is negligible. Hence we arrive at the following equation:

$$\frac{1}{r}\frac{\partial}{\partial r}\left(r\frac{\partial p^*}{\partial r}\right)=\frac{\phi\mu c_t}{\alpha_2 k(t)}\frac{\partial p^*}{\partial t} \tag{2.9}$$

However, Equation (2.9) is a nonlinear equation, but can be linearized using:

$$\frac{1}{k(t)}\frac{\partial p^*}{\partial t}=\frac{1}{k_0}\frac{\partial p^*}{\partial t^*} \tag{2.10}$$

$$t^*=\int\frac{k(t)}{k_0}dt+C=\frac{1}{k_0}\int_0^t k(t)dt \tag{2.11}$$

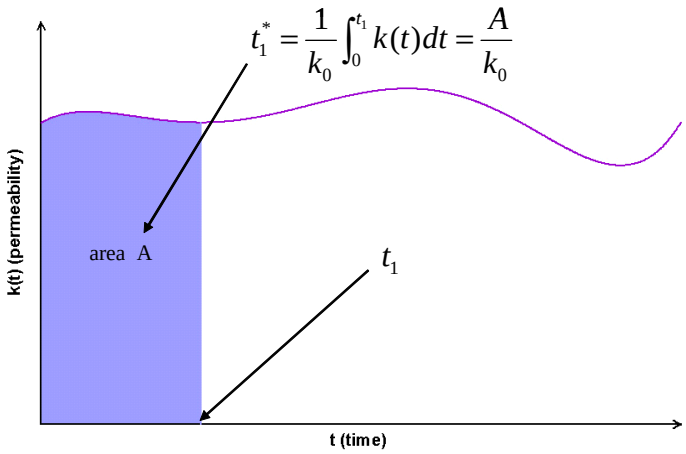

Figure 2.1: Substitute t^* for t.

The linearized equation is then:

$$\frac{1}{r}\frac{\partial}{\partial r}\left(r\frac{\partial p^*}{\partial r}\right) = \frac{\phi\mu c_t}{\alpha_2 k_0}\frac{\partial p^*}{\partial t^*} \tag{2.12}$$

This linearized equation can be solved in the usual manner for $p^*(t^*)$. For example, in infinite-acting radial flow, the solution is an exponential integral function. The final solution is then as follows, applying the initial condition and the boundary condition for the reservoir boundary:

$$p^* = C_1\int_{\infty}^{\frac{r^2}{t^*}}\left(\frac{1}{u}\exp\left(-\frac{\phi\mu c_t}{4\alpha_2}u\right)\right)du \tag{2.13}$$

After applying the well boundary condition:

$$p = \left(\frac{141.2qB\mu}{k(t)h}\right)\frac{1}{2}\int_{\frac{r^2}{t^*}}^{\infty}\left(\frac{1}{u}\exp\left(-\frac{\phi\mu c_t}{4\alpha_2 k_0}u\right)\right)du \tag{2.14}$$

Finally, the equation for the bottom hole flowing pressure is:

$$p_{wf} = p_i - p = p_i - \left(\frac{141.2qB\mu}{k(t)h}\right)\frac{1}{2}Ei\left(\frac{\phi\mu c_t}{4\alpha_2 k_0}\frac{r^2}{t^*}\right) \tag{2.15}$$

where Ei is the exponential integral solution.

2.4. Solution for Multirate Flow with Superposition Method

The previous pressure solution Equation (2.15) is for a single flow rate. The pressure response to multirate flow is described as follows:

$$p_{wf} = p_i - \frac{141.2B\mu}{k(t)h}\left(\frac{1}{2}q_1 Ei(\frac{\phi\mu c_t r_w^2}{4\alpha_2 k_0 t^*}) + \sum_{j=2}^{N}(q_j - q_{j-1})\left(\frac{1}{2}Ei(\frac{\phi\mu c_t r_w^2}{4\alpha_2 k(t_j)(t^* - t_j^*)})\right)\right) \quad \textbf{(2.16)}$$

To this solution, a skin factor, variable in time can be added:

$$p_{wfs} = p_i - \frac{141.2B\mu}{k(t)h}\left(\frac{1}{2}q_1 Ei(\frac{\phi\mu c_t r_w^2}{4\alpha_2 k_0 t^*}) + s(t) + \sum_{j=2}^{N}(q_j - q_{j-1})\left(\frac{1}{2}Ei(\frac{\phi\mu c_t r_w^2}{4\alpha_2 k(t_j)(t^* - t_j^*)}) + s(t)\right)\right) \quad \textbf{(2.17)}$$

2.5. Solution in Laplace Space

The linearized governing equation can be transferred to Laplace space. Before Laplace transformation, nondimensionlization was carried out for simplicity of variables.

$$t_D^* = \frac{\alpha_2 k_0}{\phi\mu c_t r_w^2} t^* \quad \textbf{(2.18)}$$

$$r_D = \frac{r}{r_w} \quad \textbf{(2.19)}$$

$$p_D^* = \frac{2\pi k_0 h}{\alpha_1 q B\mu} p^* \quad \textbf{(2.20)}$$

Thus, Equation (2.12) can be written:

$$\frac{1}{r_D}\frac{\partial}{\partial r_D}(r_D \frac{\partial p_D^*}{\partial r_D}) = \frac{\partial p_D^*}{\partial t_D^*} \quad \textbf{(2.21)}$$

As this point, the equation can be transferred to Laplace space.

$$£\left[\frac{1}{r_D}\frac{\partial}{\partial r_D}(r_D \frac{\partial p_D^*}{\partial r_D})\right] = £\left[\frac{\partial p_D^*}{\partial t_D^*}\right] \quad \textbf{(2.22)}$$

$$\frac{1}{r_D}\frac{\partial}{\partial r_D}(r_D \frac{\partial \bar{p}_D^*}{\partial r_D}) = s\bar{p}_D^* - p_D^*(r_D, t_D = 0) \quad \textbf{(2.23)}$$

There is an initial condition in Laplace space:

$$p_D^*(r_D, t_D = 0) = 0 \quad \textbf{(2.24)}$$

There are two boundary conditions in Laplace space.

$$\frac{1}{r_D}\frac{\partial}{\partial r_D}\left(r_D\frac{\partial \bar{p}_D^*}{\partial r_D}\right) = s\bar{p}_D^* \tag{2.25}$$

$$r_D\frac{\partial^2 \bar{p}_D^*}{\partial r_D^{\,2}} + \frac{\partial \bar{p}_D^*}{\partial r_D} - s\bar{p}_D^* r_D = 0 \tag{2.26}$$

Finally, the pressure solution in Laplace space is:

$$\bar{p}_D^* = \frac{1}{s}K_0(r_D\sqrt{s}) \tag{2.27}$$

Chapter 3

3. Verification of the Analytical Solution

The new solution with changing permeability was compared to simulation results with the commercial simulator Eclipse. Because Eclipse does not have a changing permeability model, we divided the run into small time steps and restarted the simulation after each step. In each step, an input datum of permeability was chosen as the medium value of permeability in that time step.

As a test of the analytical solution, $k(t) = 90 - 0.02t$ was used for the function of permeability. Figure 3.1 shows the permeability change in time. The blue solid line indicates the values for the function of permeability $k(t)$. The red line presents the permeability values for the Eclipse input file in each restart step.

Simulations were carried out for 1300 hours. In this time region, permeability changed from 90 md to 64 md.

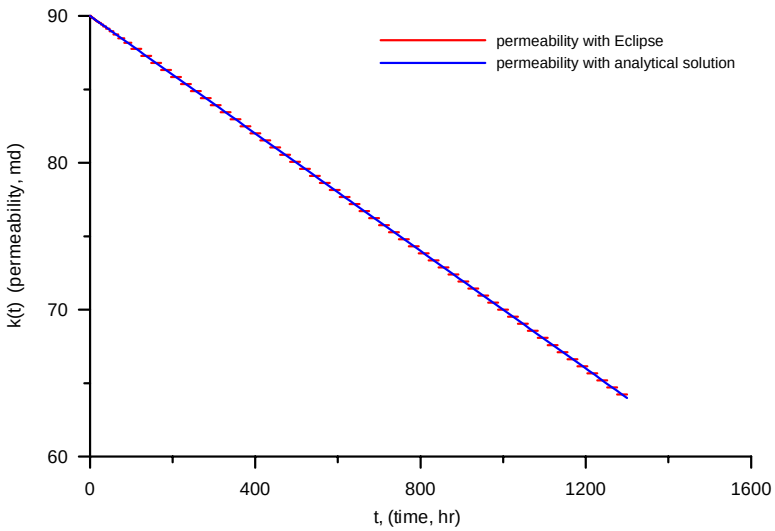

Figure 3.1: Changing permeability for the analytical solution and Eclipse runs.

In each step, the previous step's pressure data were used as the initial pressure data for the next step, along with a new value of the permeability. We considered two test cases, one of which was a single flow rate case, and the other was a multirate flow case. In both cases the simulation results (assumed to represent the correct answer) were compared to

those of the analytical solution. For reference, a constant permeability case was also considered. For the constant permeability case, the value used was 90 md.

3.1. Test Case 1: Single Flow Rate

The new solution with changing permeability was compared to the simulation results with Eclipse for a single rate flow of 1580 STB/d. other variable, in this case are listed in Table 3.1.

Table 3.1: Test case 1 properties.

μ	0.6 cp
B	1.27
h	40 ft
r_w	0.25 ft
c_t	20.0×10^{-6}
p_i	2906.0 psi
skin	0

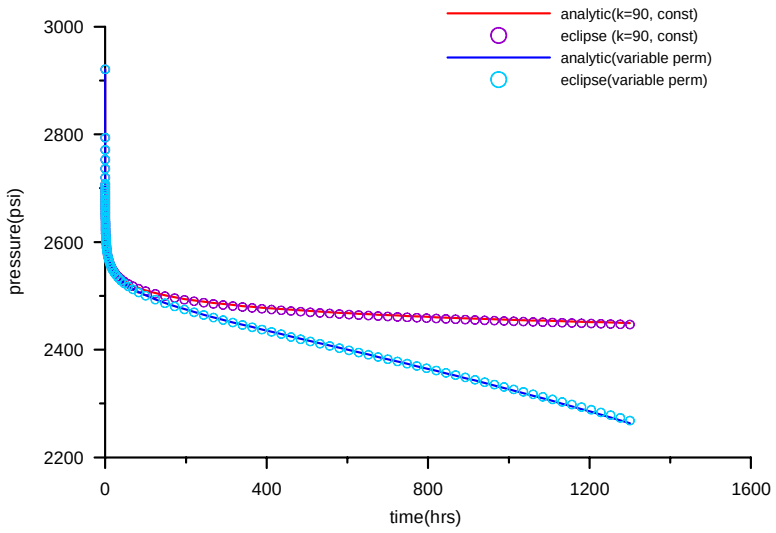

Figure 3.2: Comparing pressures from results of Eclipse runs to those of the analytical solution.

In Figure 3.2, the blue solid line shows the pressure history from the new analytical solution with changing permeability. Blue circles indicate the pressure history from the Eclipse runs. This graph shows that the result from Eclipse runs is well matched to the new analytical solution. The red solid line and purple circles are the pressure histories from constant permeability cases.

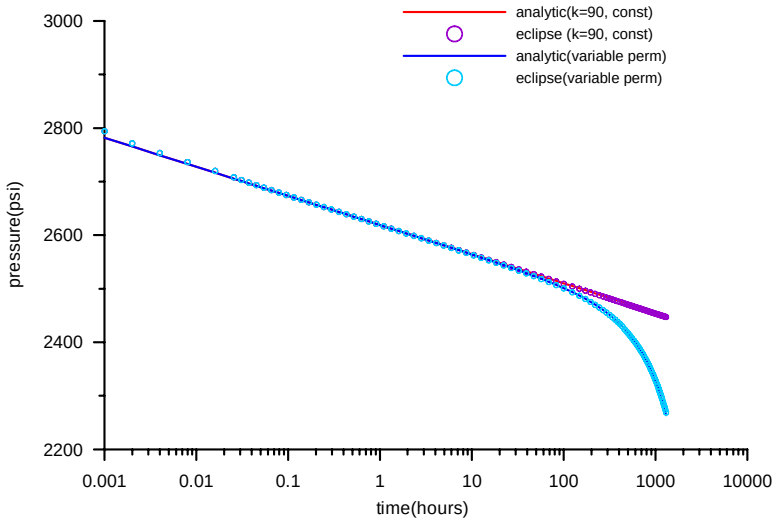

Figure 3.3: Comparing pressures from results of Eclipse runs to those of the analytical solution on a semilog scale.

The pressure histories are shown in Figure 3.3 on a semilog scale. This graph shows a good match between the Eclipse result and the new analytical solution.

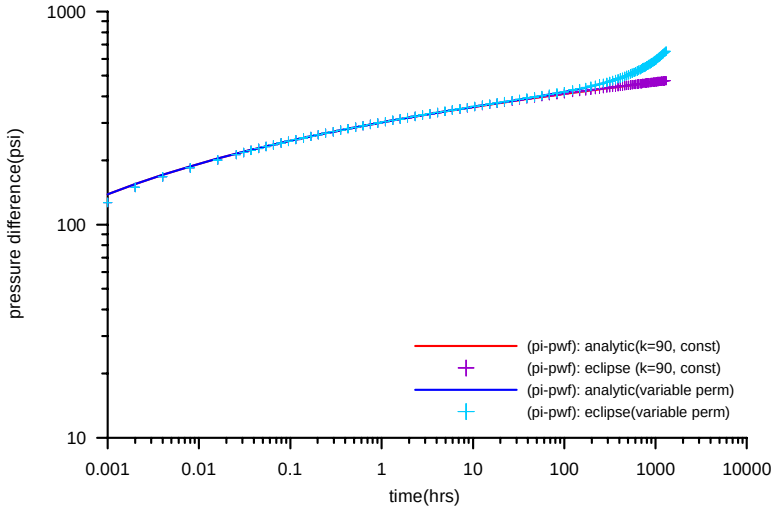

Figure 3.4: Pressure difference plot on a log-log scale.

The pressure differences, $\Delta p = p_i - p_{wf}$, are shown in Figure 3.4 on a log-log scale. This graph shows a good match between the Eclipse result and the new analytical solution on a log-log scale.

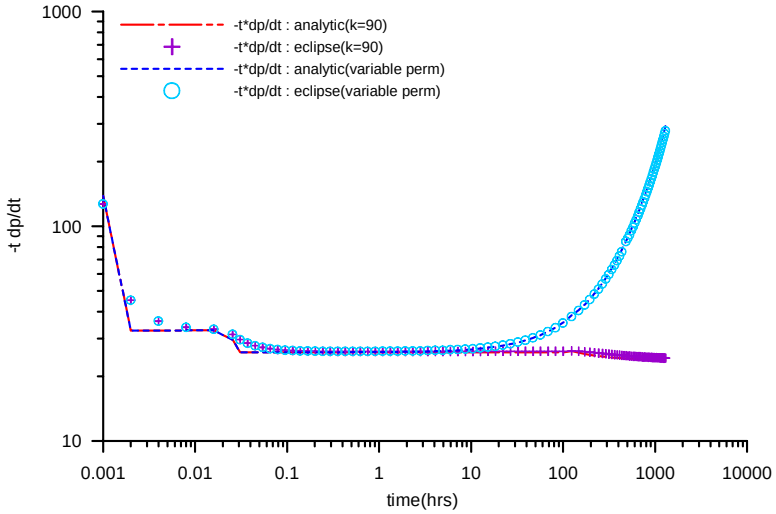

Figure 3.5: Derivative plot on a log-log scale.

The derivative plot, $t\frac{dp}{dt}$, is presented in Figure 3.5 on a log-log scale. The derivative values also show a good match between the Eclipse result and the new analytical solution. At the very early time, there are some differences, because Eclipse presents the pressure result to a numerical precision of 10^{-3}.

3.2. Test Case 2: Multirate Flow

The new solution with changing permeability was compared to the simulation results with Eclipse in multirate flow. Figure 3.6 presents the results.

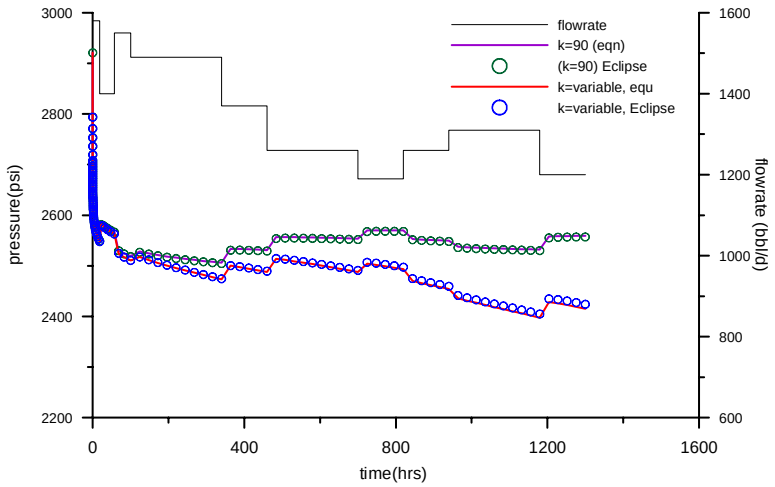

Figure 3.6: Comparing pressures from results of Eclipse runs to those of analytical solution for a multirate flow case.

In Figure 3.6, the black solid line is the flowrate. The red solid line shows the pressure history from the new analytical solution with changing permeability. Blue circles indicate the pressure history from the Eclipse runs. This graph shows that the result from Eclipse runs is well matched to the new analytical solution. The purple solid line and green circles are pressure histories from constant permeability cases with the same flowrate.

Importantly, this multirate test case confirms that the linearized changing permeability solution can correctly be superposed in time to generate variable rate solutions.

Chapter 4

4. Interpretation of Real Data

Interpretations of real data were carried out using the new changing permeability model. The real data are from a reservoir in the North Sea. Nonlinear regression was used to match the analytical model to the data.

4.1. Nonlinear Regression

The Gauss-Newton method was used for nonlinear regression.

The unknown parameters are initial permeability, initial skin factor, coefficients of the functions of permeability and skin factor, and an initial pressure. For example, when the function of permeability is $k(t) = k_0 - at$, and the function of skin factor is $s(t) = s_0 - bt$, there are five unknowns: k_0, a, s_0, b and an reservoir initial pressure p_i.

It is important to be careful about initial guesses for the function of permeability because the permeability must be positive at all time. The estimated permeability could become negative after a few iterations, unless initial guesses are proper. Figure 4.1 shows an example of negative permeability. Practically, one of the choices is that the initial guess of a is:

$$a = \frac{k_0}{t_{the\ end\ of\ data}} - \alpha \qquad \textbf{(4.1)}$$

In such a guess, α is any value that is positive and smaller than the value $\frac{k_0}{t_{the\ end\ of\ data}}$.

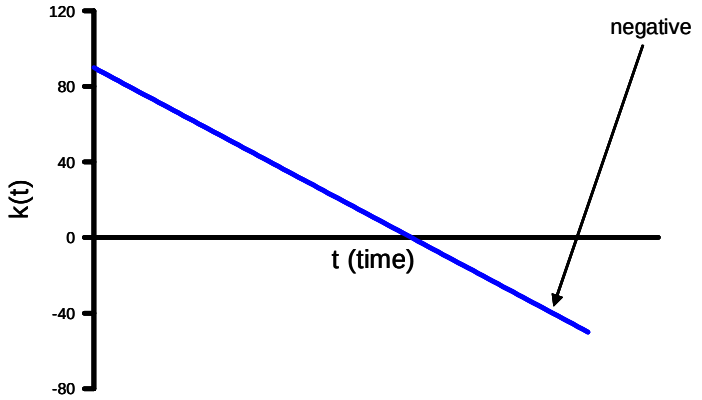

Figure 4.1: An example of negative permeability.

4.2. The Real Data Set

The total number of real pressure data points was 11,019. The data cover 20,052 hours, or about 835 days. Figure 4.2 shows the real data set which consists of pressure data and flowrate data.

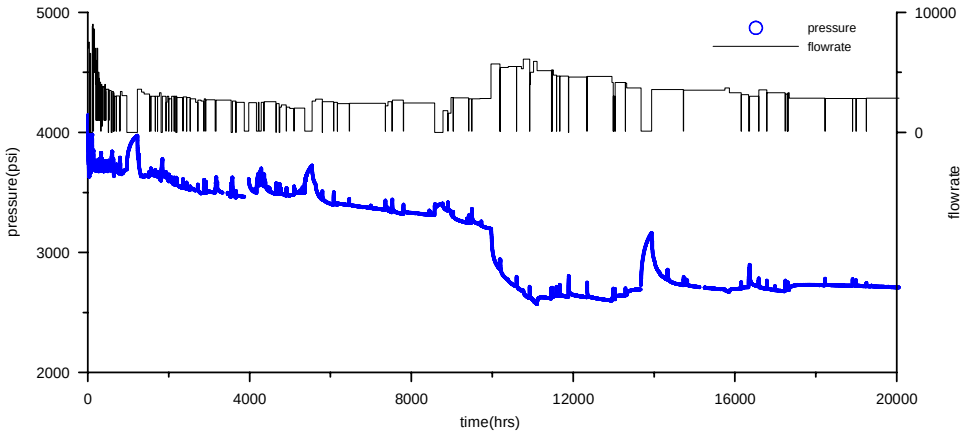

Figure 4.2: A real data set constructed by pressure and flowrate records.

The interpretations were processed by matching between real data and calculated results. The calculation was based on the new analytical solution with the changing permeability and skin factor. The calculation has two processes: inverse and forward modeling. Inverse modeling, described in the previous section, can determine the reservoir parameters, which are an initial pressure, an initial permeability, an initial skin factor, a permeability function and a skin factor function. Finally, the calculated results are presented by

forward modeling which is carried out with the best-fit parameter values determined by the inverse modeling.

The analysis used the data collected after the first 1,000 hours. There were two reasons why the first 1,000 hours were excluded. The first is that the flowrate changed frequently and the well was shut down many times during that period as shown in Figure 4.2. This may exaggerate skin effects and superposition effects in the equation for multirate flow. The second is shown in Figure 4.3. The data for the first 1,000 hours is much denser. This could influence inverse modeling, by biasing the early data over that of the other regions. Therefore, only the more uniform data after the first 1,000 hours were used for the interpretation.

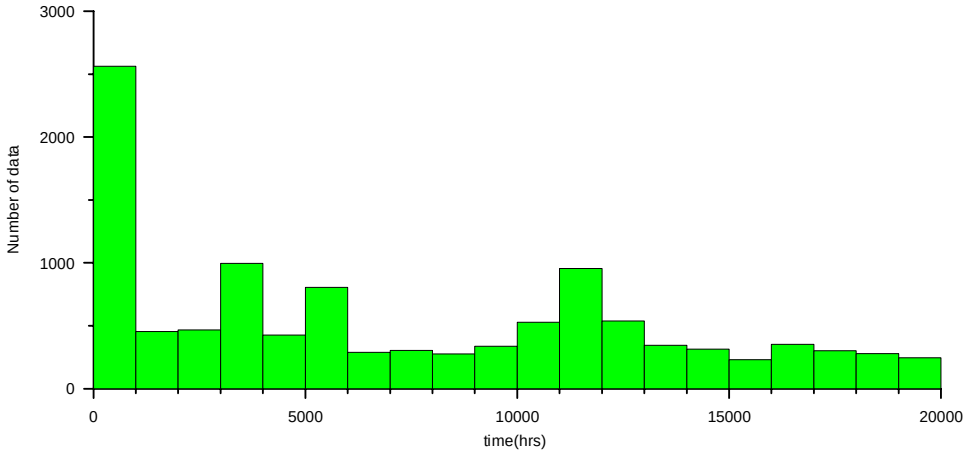

Figure 4.3: The real data distribution.

Before analysis with the new solution, a test match to the constant property solution was carried out. Figure 4.4 shows the result. The results based on the constant property solution do not match the real data set. Since the constant property solution takes the average values of permeability and skin factor, the early time and the late time differ greatly between the real data and the simulated results in particular. Clearly, the constant property solution is not appropriate for this long-term pressure data set.

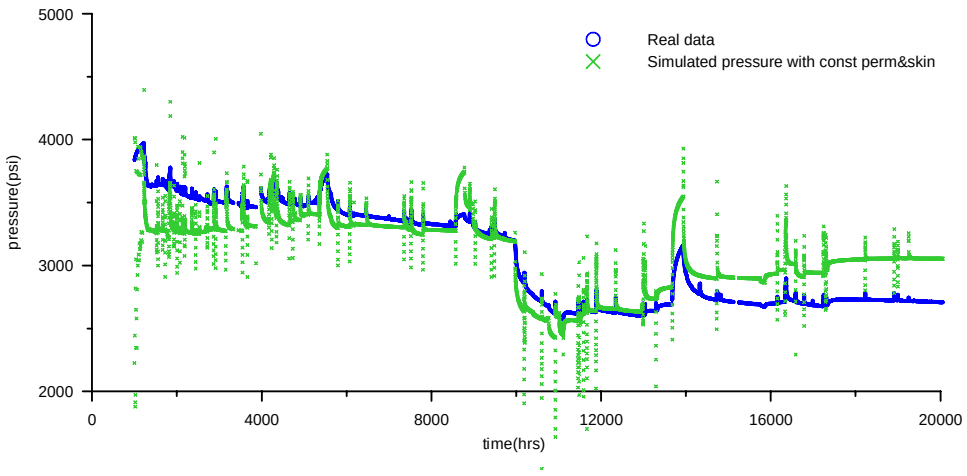

Figure 4.4: Matching the constant property solution to the real data.

4.3. Matching with a Linear Permeability Function

Matching based on the new solution with a linear permeability function was carried out. Also, a linear line function was chosen as a function of skin factor. Hence the time variation of permeability and skin were described by:

$$k = k_0 - at \quad \textbf{(4.2)}$$

$$s = s_0 - bt \quad \textbf{(4.3)}$$

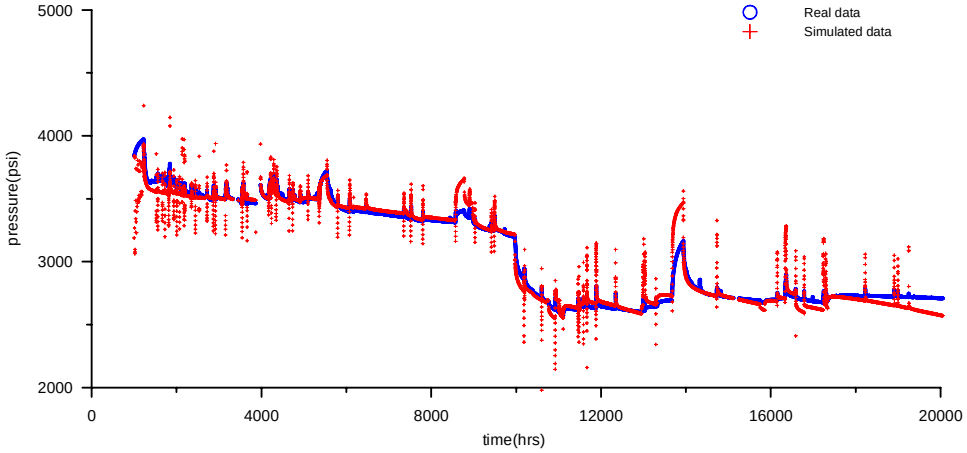

Figure 4.5: Matching with the linear permeability and skin factor functions to the real data.

Figure 4.5 presents the result of the pressure matching. Figure 4.6 shows the histories of permeability and skin factors. This result is much better than that of the constant property solution shown earlier in Figure 4.4. However, at late time, there are some differences

between the real data and the simulated results. It seems likely that the permeability and skin factor changes do not occur consistently according to a linear function.

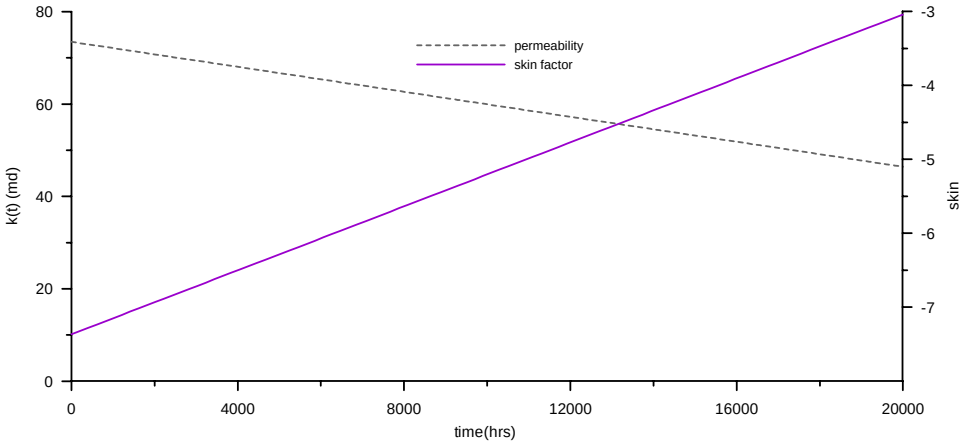

Figure 4.6: Permeability and skin factor histories.

4.4. Matching with Multiple Linear Permeability Functions

To overcome the limitation that the permeability and skin factor changes may not always occur according to just one straight line function, two different straight line functions were applied to both the permeability and the skin factor. The functions for the permeability and the skin factor were determined using the data from the first 10,000 hours. Different functions were then determined using the data after 10,000. Hence the time variation of permeability and skin were described by:

$$k = \begin{cases} k_0 - a_1 t & , t < 10{,}000 \\ k_{10{,}000} - a_2 t & , t \geq 10{,}000 \end{cases} \quad \textbf{(4.4)}$$

$$s = \begin{cases} s_0 - b_1 t & , t < 10{,}000 \\ s_{10{,}000} - b_2 t & , t \geq 10{,}000 \end{cases} \quad \textbf{(4.5)}$$

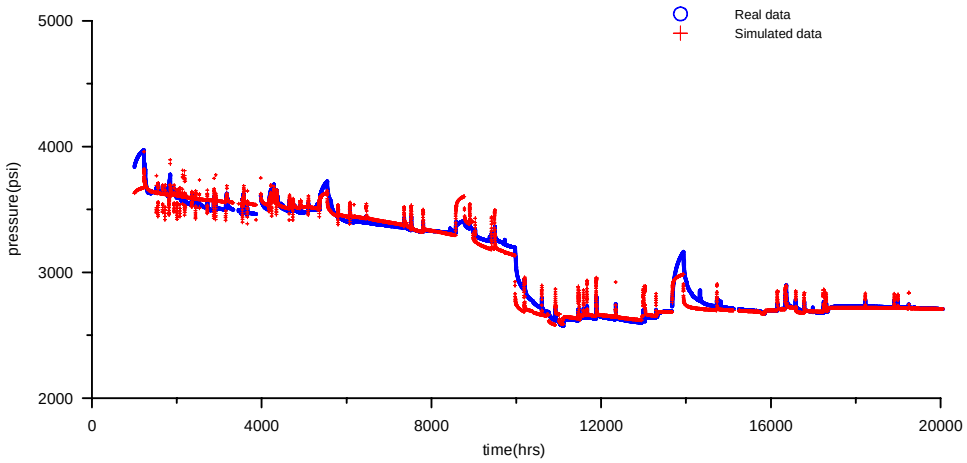

Figure 4.7: Matching with multiple linear permeability functions and skin factor functions.

Figure 4.7 presents the result of the pressure matching. Figure 4.8 shows the histories of permeability and skin factors. This result is better than the result with just one straight line function, which was shown earlier in Figure 4.5. However, in the mid time, around 10,000 hours, there are some differences between the real data and the calculated results, since the functions of the permeability and skin factor changed in this time region, which resulted in abrupt change of the values of permeability and skin factor.

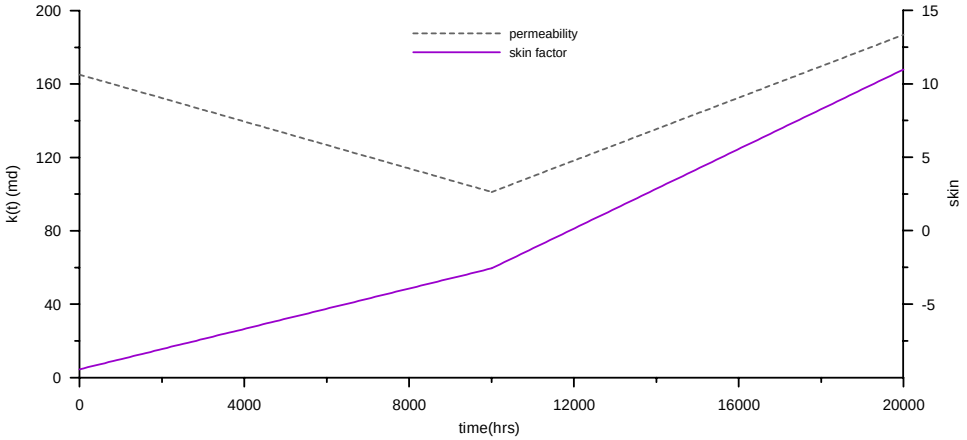

Figure 4.8: Permeability and skin factor histories.

4.5. Matching with a Quadratic Permeability Function

From Figure 4.8, there is the possibility that permeability decreases during the early time and increases after some time. Therefore, a quadratic function of the permeability is

applicable. The quadratic function of the permeability with a linear line skin factor function was applied. In this case, the time variation of permeability and skin were described by:

$$k = k_0 + c\,t + d\,t^2 \quad \textbf{(4.6)}$$

$$s = s_0 - bt \quad \textbf{(4.7)}$$

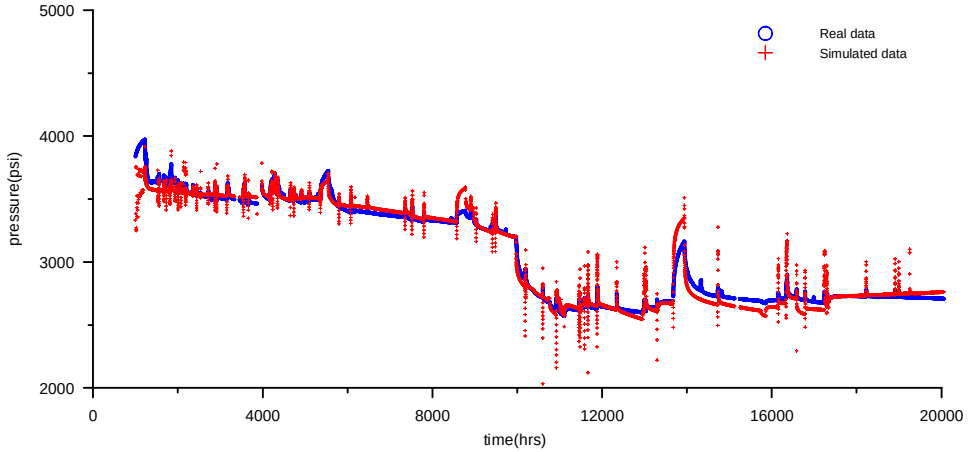

Figure 4.9: Matching with a quadratic permeability function and a linear skin factor function.

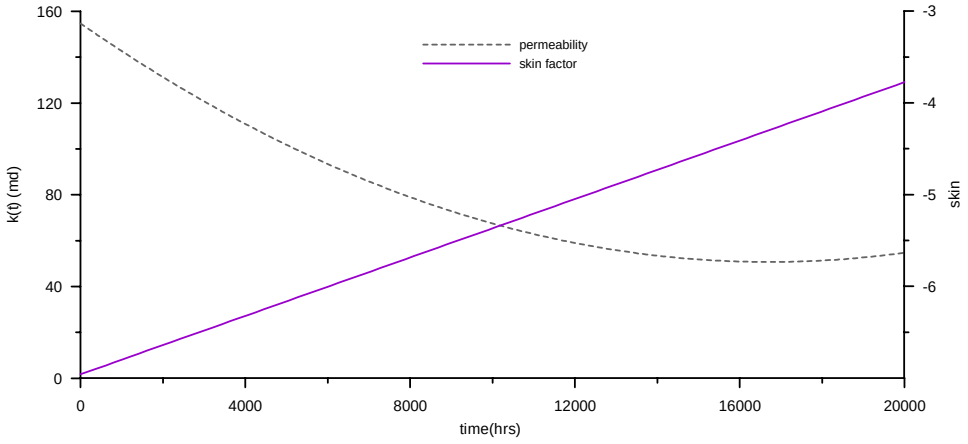

Figure 4.10: Permeability and skin factor histories.

Figure 4.9 presents the result of the pressure matching. Figure 4.10 shows the histories of permeability and skin factors. This result matches the real data well, thus demonstrating that the smoothly varying quadratic function of the permeability is a good approximation.

Chapter 5

5. Summary and Conclusion

5.1. The New Solution

The analytical solution to analyze long-term pressure data was developed in this study. This solution is for an infinite-acting radial flow (IARF) reservoir with changing permeability and skin factor. Figure 5.1 shows the new solution be more precise to analyze real data than the constant property solution.

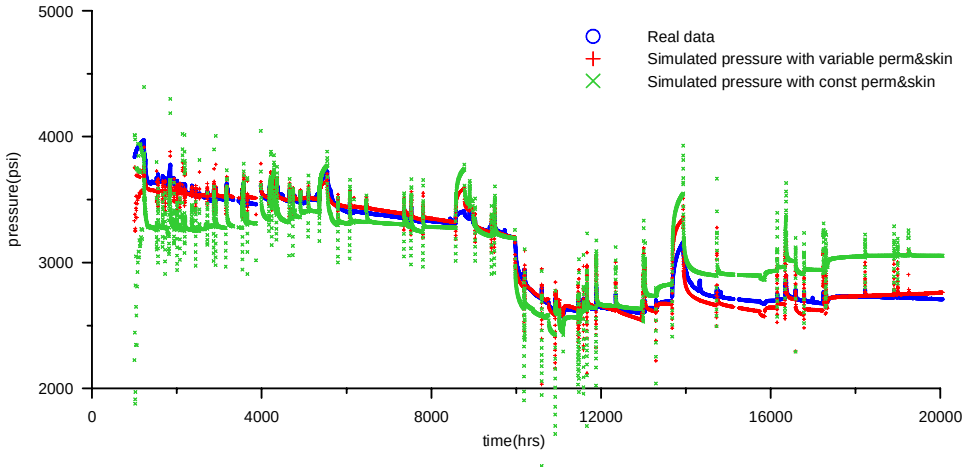

Figure 5.1: Comparing the new solution with a quadratic permeability function and the constant property solution to the real data.

The new solution was verified for numerical accuracy by comparison with a numerical simulator, and was confirmed to represent a multirate flow history using superposition.

5.2. Future Work

There are two considerations for future work.

The new solution is based on the assumption that permeability is changing very slowly in time. In this paper, the exact range of “very slowly” was not described. In future work this should be investigated to come up with a more precise characterization.

The solution for long-term pressure data developed in this study is for infinite-acting radial flow reservoirs. The solutions for other types of reservoirs are needed. The linearization variable, t^* which is described in Chapter 2 should be applicable for other type of reservoirs.

Nomenclature

k_0 = initial permeability
s_0 = initial skin factor
c_t = total compressibility
B = formation volume factor
μ = viscosity
h = thickness of a reservoir
r_w = well radius
p_{wf} = well bottom hole flowing pressure
p_i = initial pressure
α_1 = 141.2(2π)
α_2 = 0.000264

References

Athichanagorn, S., 1999, “Development of an Interpretation Methodology for Long-Term Pressure Data from Permanent Downhole Gauges”, PhD dissertation, Stanford University.

Khong, C. K., 2001, “Permanent Downhole Gauge Data Interpretation”, MS report, Stanford University.